CONF-8510168--7

IN-SITU STUDY OF CASCADE DEFECTS IN SILVER BY SIMULTANEOUS TRANSMISSION ELECTRON MICROSCOPY AND ELECTRICAL RESISTIVITY MEASUREMENTS AT LOW TEMPERATURES*

K. Haga**, Wayne E. King, K. L. Merkle and M. Meshii**
**Department of Materials Science and Engineering
Northwestern University, Evanston, IL 60201 and
Materials Science and Technology Division
Argonne National Laboratory, Argonne, IL 60439

CONF-8510168--7

DE86 005561

December 1985

Presented at the Symposium on Irradiation Effects Associated with Ion Implantation at the 1985 TMS-AIME Fall Meeting in Toronto, the proceedings of which will be published as a special issue of the Journal of Nuclear Instruments and Methods in Physics Research -- Section B: Beam Interactions with Materials and Atoms. (October 14-15, 1985)
*Work supported by the National Science Foundation and the U. S. Department of Energy, BES-Materials Sciences, under Contract W-31-109-Eng-38.

IN-SITU STUDY OF CASCADE DEFECTS IN SILVER BY SIMULTANEOUS TRANSMISSION ELECTRON MICROSCOPY AND ELECTRICAL RESISTIVITY MEASUREMENTS AT LOW TEMPERATURES*

K. Haga**, Wayne E. King, K. L. Merkle and M. Meshii**
**Department of Materials Science and Engineering
Northwestern University, Evanston, IL 60201 and
Materials Science and Technology Division
Argonne National Laboratory, Argonne, IL 60439

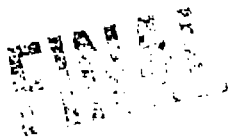

December 1985

Presented at the Symposium on Irradiation Effects Associated with Ion Implantation at the 1985 TMS-AIME Fall Meeting in Toronto, the proceedings of which will be published as a special issue of the Journal of Nuclear Instruments and Methods in Physics Research -- Section B: Beam Interactions with Materials and Atoms. (October 14-15, 1985)
*Work supported by the National Science Foundation and the U. S. Department of Energy, BES-Materials Sciences, under Contract W-31-109-Eng-38.

In-Situ Study of Cascade Defects in Silver by Simultaneous Transmission Electron Microscopy and Electrical Resistivity Measurements at Low Temperatures*

K. Haga**, Wayne E. King+, K. L. Merkle+ and M. Meshii**

**Department of Materials Science and Engineering, Northwestern University, Evanston, IL 60201, USA

+Materials Science and Technology Division, Argonne National Laboratory, Argonne, IL 60439, USA

A helium-cooled double-tilt specimen stage for transmission electron microscopy (TEM) with the capability of simultaneous electrical resistivity measurements was constructed and used to study defect-production, migration, clustering and recovery processes in ion-irradiated silver. Vacuum-evaporated thin film specimens were irradiated with 1 MeV Kr^+-ions up to a dose of 4.0×10^{10} ions/cm^2, at T = 10 K in the microscope, using the HVEM-tandem accelerator ion beam interface system in the Argonne National Laboratory Electron Microscopy Center. Cascade defect formation during ion bombardment at the low temperature was directly observed both by TEM and electrical resistivity measurements. Ion bombardment created groups of defect clusters with strong strain fields which gave rise to TEM contrast. The specimen resistivity was increased by 16% during the irradiation. Subsequent microstructural changes and resistivity recovery during isochronal annealing were monitored up to room temperature. 58.3% of the irradiation induced resistivity was recovered, while significant reduction in the size of black spot defect clusters was observed by TEM. A small fraction of clusters disappeared, while no nucleation of new defect clusters was observed.

*Work supported by the National Science Foundation and the U.S. Department of Energy, BES-Materials Sciences, under Contract W-31-109-Eng-38.

1. Introduction

In many metals, vacancy clusters have been observed in individual cascades introduced by heavy-ion or fast neutron irradiation using TEM techniques [1-4]. However, the detailed mechanisms of vacancy cluster formation, defect structure around the vacancy clusters and especially the behavior of free defects such as interstitial atoms within cascades are not well known. In the past, irradiation and TEM observation were carried out separately and most post-irradiation TEM observations were done at room temperature. Recently, the HVEM-tandem accelerator ion beam interface system in the Argonne National Laboratory Electron Microscopy Center has provided the opportunity for in-situ ion irradiation experiments and simultaneous TEM observations in a high voltage electron microscope [5-7]. Using special specimen stages, it has become possible to examine ion irradiation effects over a wide range of specimen temperatures.

In our previous work on silver and gold irradiated with 20-140 keV Kr^+-ions, it was found that visible vacancy clusters were formed in both materials even at temperatures below 10 K where no thermal migration of interstitials or vacancies is expected [8]. Because our first low temperature stage had only one specimen-tilt axis, these studies were limited by the inability to reach every crystallographic orientation required for defect analysis and stereo viewing of the defect structure. Hence, we have constructed two side-entry helium-cooled double-tilt specimen stages. One of the double-tilt stages is equipped for simultaneous electrical resistivity measurements of TEM specimens and also with a heater to facilitate specimen temperature cycling experiments such as isochronal annealing. Electrical resistivity measurements com-

plement TEM observations by providing information on submicroscopic defects, the existence of which has been indicated by resistivity measurements [9] and x-ray diffuse scattering measurements [10,11].

The new helium-cooled specimen stages in combination with the ion beam interface system are useful to study not only defect behaviors in metals but also irradiation induced metastable phases at low temperatures. In this paper, we describe the helium-cooled double-tilt specimen stage with the capability of simultaneous electrical resistivity measurements and results on silver irradiated at T = 10K with 1 MeV Kr^+-ions and then annealed isochronally up to room temperature. This work represents the first attempt to correlate TEM observations with electrical resistivity measurements directly on the same specimen at low temperature.

2. Specimen stage

In the past, a number of helium-cooled TEM specimen stages were constructed to meet various requirements (e.g. see ref. 12 and 13). We have previously constructed a single-tilt stage for in-situ electrical-resistivity measurements in the high voltage electron microscope [14]. Since TEM image contrast of crystalline materials is sensitive to the specimen orientation and since an ability to obtain different diffraction conditions and different crystallographic directions is essential in defect structure analysis, a specimen stage with two orthogonal tilt axes is desirable.

For accurate measurements of small changes in electrical resistivity due to irradiation induced defects, it is necessary to carry out measurements at a temperature where the phonon contribution to the

resistivity is negligible. For most metals resistivity becomes insensitive to temperature below 10 K. In addition, no defects are mobile in silver at this temperature.

Another requirement is rapid cycling of specimen temperature which makes in-situ isochronal annealing possible in a short time over a wide temperature range. This necessitates a small heater attached very close to the specimen in addition to a helium flow-rate control system for specimen temperature regulation.

We constructed a specimen stage which meets these requirements for the 1.2 MeV KRATOS-AEI EM7 electron microscope at Argonne National Laboratory. The tip of the side-entry stage is shown in fig. 1. X-tilt around the axis of the stage is provided by a drive device outside of the microscope column and ranges to $\pm 60^{\circ}$. Y-tilt is obtained by rotating the wheel on the specimen tilt cup through a friction drive using a pushing pin. This gives a Y-tilt range of $\pm 30^{\circ}$. The specimen tilt cup is made of sapphire with resistor ink printed on it as a heater. A copper insert accommodates a threaded ring which holds down the specimen holder disk achieving good thermal contact between the disk and the specimen tilt cup. Two copper braids are attached to this copper insert using indium solder and are mechanically clamped at the other end onto the copper body of the tip. This thermal connection is good enough to cool the specimen holder disk to below 10 K. On the other hand, the thermal contact is weak enough to effectively isolate the specimen tilt cup from the tip body when the heater is on and thus allows only the cup to warm up rapidly. Keeping the temperature of the tip body near 10 K with constant flow of liquid helium, we are able to warm up the specimen holder disk to 300 K within 7 minutes and cool it down to 10 K within 5

minutes. During warming up, the specimen orientation changes somewhat, due to the thermal expansions of the specimen stage and the specimen. The original specimen orientation is, however, restored by itself during cooling down. Thus, almost no stage readjustments are necessary for taking micrographs under an identical diffraction condition at low temperature following each isochronal annealing cycle. The liquid helium consumption rate for the constant flow is about 4.5 liters per hour and the heater power to achieve 300 K is approximately 1.5 W. The tip body is cooled through a copper screen heat exchanger by liquid or gaseous helium delivered by a helium transfer tube. The stage tip is covered with a cold shield which is cooled by the return flow of helium [14]. The cold shield prevents radiation heat flow to the stage from ambient and also traps residual gases in the microscope vacuum thus minimizing their condensation on the specimen.

The temperature of the tip body is monitored using a commercial platinum resistance thermometer [15]. The specimen temperature is monitored by a platinum resistance thermometer printed on the sapphire specimen holder disk. This thermometer is calibrated following each experiment. Electrical leads to the thermometers and to the specimen are introduced into the vacuum-side of the stage through an epoxy seal [16]. To accomplish the electrical connections to the specimen holder disk, two sapphire connection plates with printed gold pads are used. The first plate is stationary and carries the termination pads of the wires going through the epoxy seal. Flexible connections are made from this first plate to a second plate. The second plate is movable and a part of the Y-tilt friction drive. Electrical leads to the heater are introduced in the same way and terminated on the first connection plate.

Leads between the first plate and the heater are inside the copper cooling-braids. All copper parts are made of OFHC copper and gold-plated [17].

3. Experimental procedure

Single crystal silver [18] films were vapor deposited onto single crystal sodium chloride (NaCl) substrates under a vacuum of 7×10^{-5} Pa using a similar technique to that described by Schober [19]. The specimen thickness as determined by gravimetry was 110 ± 1 nm. The specimen film normal was [001]. After evaporation, the NaCl substrates were dissolved in distilled water and the silver films were mounted on sapphire specimen holder disks. Each sapphire disk was prepared previously with silver electrical contact pads and a platinum strip (used as a temperature sensing element) using thick film metallic inks. The back sides of the disks which face electron and ion beams were coated with silver ink to avoid charging effects. Each silver film on a sapphire disk was then covered with a molybdenum ion milling mask of the desired specimen geometry. The unmasked area of the film was sputtered away by Ar^+-ion bombardment in vacuum. After ion-milling, several disks were wrapped together in a silver foil and mounted on a tungsten boat in a vacuum chamber. The boat was then resistance heated under a vacuum of 7×10^{-5} Pa. Specimens were annealed at about 500° C for 1 hour and then cooled to room temperature over 2 hours. One of the disks was then mounted in the specimen tilt cup of the specimen stage and eight bare gold wires were attached to the silver connection pads using a thermosonic wire bonder. A silver specimen mounted on a sapphire specimen holder disk is shown in fig. 2. After insertion into the microscope

column and after the vacuum reached a pressure below 10^{-4} Pa the stage was cooled down to below 10 K. Initial cooling of the flow cryostat system takes about 30 minutes.

The electrical resistance measurements were done using the standard 4-probe dc-technique. During resistance measurements, the microscope objective lens current was turned off to avoid interference of the lens magnetic field with the dc measurements. The geometry factor f that relates resistance to resistivity was calculated from resistances measured at room temperature (R_{RT}) and at temperatures below 10 K ($R_{<10K}$) from the relation:

$$f = \rho_{iRT}/(1.004R_{RT} - R_{<10K}).$$

The intrinsic resistivity of silver at room temperature ρ_{iRT} is given by Matula [20]. The factor 1.004 accounts for the thermal contraction of the specimen during cooling.

TEM observations were carried out outside of the electrical resistivity gauge area, since it was found that the specimen resistivity increases slightly if the gauge area of the specimen is irradiated with electrons even when an electron energy of 400 keV is used, which is well below the displacement threshold electron energy of 770 keV reported by Kiritani [21]. The electrical resistivity is very sensitive to any small changes in defect population caused by subthreshold electron damage or to electron beam heating. Fig. 3 shows a low magnification electron micrograph of the specimen indicating the electrical resistivity gauge area and the TEM observation area.

The specimen was irradiated with 1 MeV Kr^{+}-ions at T = 10 K in the high voltage electron microscope using the ion-beam interface system to a dose of 4.0×10^{10} ions/cm^2. Details of the irradiation technique

have been described elsewhere [5,6,8,22]. After the irradiation, an isochronal annealing run was carried out using a holding time of 600 sec. Details of the annealing program and results are given in table 1.

4. Results and discussion

Since the purpose of this work was the study of defect structure in individual cascades, the rather low ion dose of 4.0×10^{10} ions/cm^2 was chosen. This gives an average distance between ion impacts of 50 nm and therefore the complications that might arise from superposition of successive cascades can be neglected in this work.

Fig. 4 shows a series of dark field micrographs of the specimen taken under the two beam dynamical condition with the electron energy of 400 keV, the reflection vector $\underset{\sim}{g} = 200$, foil orientation $Z \simeq 001$. All micrographs were taken at 10 K. Fig. 4(a) shows the observation area before irradiation. Microstructural changes in the area were followed during the irradiation and the isochronal annealing. Fig. 4(b) is a micrograph taken immediately after the irradiation. Many black spot defect clusters were created during irradiation. The black spots occur in bunches, i.e. in general, several individual spots are close to one another. Some of the larger spots are thought to be composed of several subcascade defects. In some cases, it was difficult to resolve subcascade structure within each individual cascade, since the electron micrographs were a projection in a direction only 18° from the incident ion beam direction. An example of well resolved subcascade structure is seen near the bottom right corner of fig. 4(b), which resulted from the rare event of large angle scattering. Comparison of the ion dose and the number of defect clusters produced also indicates that more than one black spot was

produced per incident ion. Subcascade formation is quite pronounced under 1 MeV Kr^+ ion irradiation of silver. A few defects which show black-white contrast are located close to the specimen surfaces [23]. Based on the results of our early work [8], these defects are expected to be of vacancy type.

Figs. 4(c),(d) and (e) show the microstructural evolution during annealing for 10 minutes at 52 K, 117 K, and 198 K, respectively. All micrographs were taken at T = 10 K. The overall trend of the annealing process which is seen in these micrographs is that the total area occupied by black spots and the size of most spots decrease gradually. The predominant feature seems to be the shrinkage in size of individual black spots. Also, some of the subcascade defect clusters disappeared completely. It is possible that loss of some dislocation loops is due to their glide to the surface. In a few instances the movement of defect clusters is seen, suggesting dislocation loop glide. The observed directions of defect movement were parallel to projections of <110> directions onto the (001) image plane.

Bright-field electron micrographs of the same area are shown in fig. 5. These micrographs were taken with the reflection vector $\underline{g} = \bar{2}00$, slightly deviated from the exact dynamical condition to achieve the high contrast. Fig. 5(a) is a micrograph taken immediately after the irradiation. Fig. 5(b) shows the area after annealing at 198 K for 10 minutes. The micrograph taken after the final anneal at 293 K for 10 minutes is fig. 5(c). The reduction in the size of black spots is clearly seen from these figures. During the annealing no nucleation of new defect clusters was observed. However, after the anneal at 293 K a fine-scale modulation of the background intensity was observed. It

appears as though this is associated with a change in surface morphology.

The results of the electrical resistivity recovery during the same isochronal annealing run are shown in table 1 and fig. 6. After the annealing at 52 K, 6.5 % of the irradiation induced resistivity was recovered. This small stage I recovery is consistent with the cases of fast neutron irradiation [24] and 720 keV Bi^{+++} irradiation [25]. The corresponding microstructural change is also small (figs. 4(b) and 4(c)). After the second annealing at 117 K which is in stage II, the total resistivity recovery reached 18.2 %. The reduction in the size of black spots is seen in fig. 4(d) compared with fig. 4(c). The third annealing was carried out at 198 K which was close to the stage III recovery peak at 210 K [24,25]. An additional recovery in the electrical resistivity was more than 20% at this temperature. However, the microstructural change seen between fig. 4(d) and (e) is not evident. After final annealing at 293 K, which corresponds to the end of stage III. 58.3% of the irradiation induced resistivity was recovered. This recovery is somewhat smaller compared with 720 keV Bi^{+++} irradiation of silver, in which a total recovery of 72% was observed [25]. This difference might be partly due to the difference in the specimen thickness. The thickness of the specimen used in the present work is about one-half of that in the work by Averback et.al. [25]. A higher fraction of interstitials might have been lost to the surface, leaving more vacancy-type defects in our specimen. In fast neutron irradiated silver, a total recovery of 82% was observed up to 293 K [24]. The specimen was a polycrystalline wire 5 cm long with a diameter of 0.25 mm [24].

How can we understand the present observations in terms of defect production and rearrangement and annealing of defect clusters in energetic cascades? First, the fact that practically all of the cascades produced visible defect clusters in irradiation of silver at 10 K indicates that the depleted zones are compact enough to contain initially a high energy density which causes defect rearrangement during the thermal spike phase of cascade evolution [8] and are also large enough in size to produce collapsed structures that generate visible contrasts.

The small amount of stage I recovery indicates that the collapse process leaves almost no isolated Frenkel pairs and free interstitial atoms. Stage I recovery can largely be accounted for by the recombination of isolated Frenkel pairs created by low energy recoils between energetic subcascades. Practically all of the interstitial defects are clustered. The clustering process is thought to take place during the later stages of the cascade evolution. The interstitial clusters are presumed to be arranged at the periphery of the depleted zones and are generally too small to be visible in the TEM micrographs.

The fact that a gradual reduction of the size of the black spots is observed during annealing, indicates that some of the interstitial clusters must become mobile and can recombine with the vacancy clusters that are formed in the depleted zone. The enhanced mobility of submicroscopic interstitial clusters between 52 K and 117 K is consistent with the HVEM observation of electron irradiated copper by Jäger, et. al. [26]. In some cases, however, the apparent shrinkage of black spots could be due to loss of some overlapping subcascades by dislocation loop glide to the surface. The gradual reduction of the size of the black spots seems commensurate with the amount of resistivity recovery.

The present observations have shown correlation between the resistivity recovery and the microstructural changes in energetic cascades. Further work will concentrate on a quantification of the observed reduction in defect sizes and numbers and will also address the question of the influence of electron subthreshold damage on cascade structures.

5. Summary

A helium-cooled double-tilt specimen stage for transmission electron microscopy with the capability of simultaneous electrical resistivity measurement was constructed. It was used to correlate microstructural evolution with electrical resistivity recovery in a silver specimen during isochronal annealing after 1 MeV Kr^{+}-ion irradiation up to 4.0×10^{10} ions/cm^2. Cascade defect cluster formation during ion bombardment at T = 10 K was directly observed. Groups of defects formed in subcascades were observed.

During annealing, the total area of defects and the size of individual spots were reduced gradually suggesting the shrinkage of vacancy clusters due to recombination with submicroscopic interstitial clusters and the loss of subcascade defects through dislocation loop glide. Stage I recovery was less than 6.5% indicating the retention of very few single Frenkel pairs and free interstitial atoms in energetic cascades. During the isochronal annealing up to room temperature, 58.3% of the irradiation induced electrical resistivity was recovered. This resistivity recovery seems commensurate with the amount of the reduction in the total area of defects. No nucleation of new defect clusters was observed.

Acknowledgements

The authors gratefully acknowledge the technical support of the Argonne National Laboratory Electron Microscopy Center staff. This work has been supported by the Metallurgy Program, Metallurgy and Materials Science Section, Division of Materials Research, National Science Foundation under grant number DMR-8411178 and by the U. S. Department of Energy.

References

[1] M. Kiritani, J. Nucl. Mater. 133 & 134 (1985) 85.

[2] B. L. Eyre and C. A. English, in Point Defects and Defect Interactions in Metals, ed. by J. Takamura, M. Doyama, and M. Kiritani, Univ. of Tokyo Press, Tokyo (1982) 799.

[3] W. Jäger, J. Microsc. Spectrosc. Electron. 6 (1981) 437.

[4] K. L. Merkle, in Radiation Damage in Metals, American Society for Metals, Metals Park, OH (1976) 58.

[5] A. Taylor, J. R. Wallace, E. A. Ryan, A. Philippides and J. R. Wrobel, Nucl. Instr. and Meth. 189 (1981) 211.

[6] A. Taylor, E. A. Ryan, A. Philippides and J. R. Wallace, Mater. Sci. Eng. 69 (1985) 457.

[7] A. Taylor and E. A. Ryan, Nucl. Instr. and Meth. B 10/11 (1985) 687.

[8] K. Haga, A. C. Baily, Wayne E. King, K. L. Merkle and M. Meshii, in Proc. of Seventh International Conference on High Voltage Electron Microscopy, ed. by R. M. Fisher, R. Gronsky and K. H. Westmacott, Univ. of California, August 16-19 (1983) 139 in LBL-16031.

[9] R. S. Averback, J. Nucl. Mater. 108 & 109 (1982) 33.

[10] B. C. Larson and F. W. Young, Jr., in Ref. 2, p. 679.

[11] B. C. Larson, T. S. Noggle and J. F. Barhorst, in Mat. Res. Soc. Symp. Proc. 41 (1985) 25.

[12] E. P. Butler and K. F. Hale, Practical Methods in Electron Microscopy, Vol. 9, ed. A. M. Glauert (North Holland, Amsterdam, 1981).

[13] H. G. Heide, Ultramicroscopy 10 (1982) 125.

[14] W. E. King, in Electron microscopy 1978, Vol. 1, ed. J. M. Sturgess, Microscopical Society of Canada (1978) 68.

[15] Manufacturer calibrated platinum resistance temperature sensors were supplied by Rosemount, Inc., P.O. Box 35129, Minneapolis, MN 55435.

[16] Epoxy casting resin STYCAST 2850 GT was supplied by Emerson & Cuming, W. R. Grace & Co. 869 Washington St., Canton, MA 02021.

[17] Most of the metal parts were machined by Gatan, Inc., 780 Commonwealth Dr., Warrendale, PA 15086, all of the sapphire parts were machined by Insaco, Inc., P.O. Box 460, Quakertown, PA 18951 and thick film inks were supplied by Engelhard Co., 1 West Central Ave., East Newark, NJ 07029.

[18] 6-9 grade high purity silver (shot) was supplied by Cominco American Inc., Bldg. 101, Spokane Industrial Park, Spokane, WA 99216.

[19] T. Schober, J. Appl. Phys. 40 (1969) 4658.

[20] R. A. Matula, J. Physical and Chemical Reference Data 8 (1979) 1147.

[21] M. Kiritani, in Progress in the Study of Point Defects, ed. by M. Doyama and Sho Yoshida, Univ. Tokyo Press (1977) 247.

[22] R. L. Lyles, K. L. Merkle and P. Okamoto, in Proc. Fifth Int. Conf.

on High Voltage Electron Microscopy, Kyoto, Japan, ed. by T. Imura and H. Hashimoto (Japanese Society of Electron microscopy, Tokyo, 1977) 83.

[23] M. Rühle, in Radiation Damage in Reactor Materials, IAEA, Vienna, Vol. 1 (1969) 113.

[24] J. A. Horak and T. H. Blewitt, J. Nucl. Mater. 49 (1973) 161.

[25] R. S. Averback, L. J. Thompson and K. L. Merkle, J. Nucl. Mater. 69 & 70 (1978) 714.

[26] W. Jäger, W. Frank and K. Urban, Radiat. Eff. 46 (1980) 47.

Table 1. Electrical resistivity recovery in silver during isochronal annealing after 1 MeV Kr^+ irradiation

Annealing step	Temperature (K)	Warming time (sec)	Annealing time (sec)	Cooling time (sec)	$\Delta\rho$ (nΩcm)	Total recovery* (%)
1	52	180	600	30	13.01	6.5
2	117	300	600	30	11.38	18.2
3	198	300	600	90	8.50	38.9
4	293	4560**	600	300	5.80	58.3

*total recovery (%) = 100 $(\Delta\rho_{IRRAD}-\Delta\rho)/\Delta\rho_{IRRAD}$, $\Delta\rho_{IRRAD}$ = 13.91 x 10^{-9} Ωcm for 4.0 x 10^{10} ions/cm^2.

**For this particular run, the heater power supply did not work properly.

Figure Captions

Figure 1 Detailed drawing of the tip of the helium cooled double tilt TEM specimen stage with the capability of electrical resistivity measurement: the end of the helium transfer tube is positioned without contact within the heat exchanger made of copper screen.

Figure 2 Silver specimen mounted on a sapphire disk of 4 mm diameter and 0.25 mm thickness with 0.6 mm diameter aperture. The 0.3 mm wide band in the form of half-circle is a platinum resistance thermometer printed on the sapphire disk; 8 bare gold wires (50 μm diameter) are attached to silver connection pads using a thermosonic wire bonder.

Figure 3 Low magnification electron micrograph of the specimen: (1) TEM observation area, (2) electrical resistivity gauge area, (3), (4) current leads, (5),(6) potential leads, (7) aperture edge of the sapphire specimen holder disk.

Figure 4 Dark-field electron micrographs of a (001) silver specimen irradiated at T = 10 K with 1 MeV Kr^+-ions to a dose of 4.0×10^{10} ions/cm^2 and then annealed isochronally. All micrographs were taken at T = 10 K, electron energy of 400 keV, $\underline{g} = 200$, $W \tilde{} 0$: (a) before the irradiation, (b) immediately after the irradiation, (c) after annealed at 52 K for 10 min., (d) after annealed at 117 K for 10 min., (e) after annealed at 198 K for 10 min. Arrowheads indicate examples of spot shrinkage, circles indicate examples of defect disappearance, and arrows indicate examples of defect

movement. The defects are marked before the change occurs. The defect reaction can be observed by comparing the marked figure with the next figure.

Figure 5 Bright-field electron micrographs of the same specimen as fig. 4. All micrographs were taken at T = 10 K, electron energy of 400 keV, $\underline{g} = \bar{2}00$, slightly deviated from the exact dynamical condition to achieve the high contrast: (a) immediately after the irradiation, (b) after annealed at 198 K for 10 min., (c) after the final anneal at 293 K for 10 min.

Figure 6 Electrical resistivity recovery in the same specimen as figs. 4 and 5 during isochronal annealing after 1 MeV Kr^{+}-ion irradiation to a dose of 4.0×10^{10} ions/cm^2.

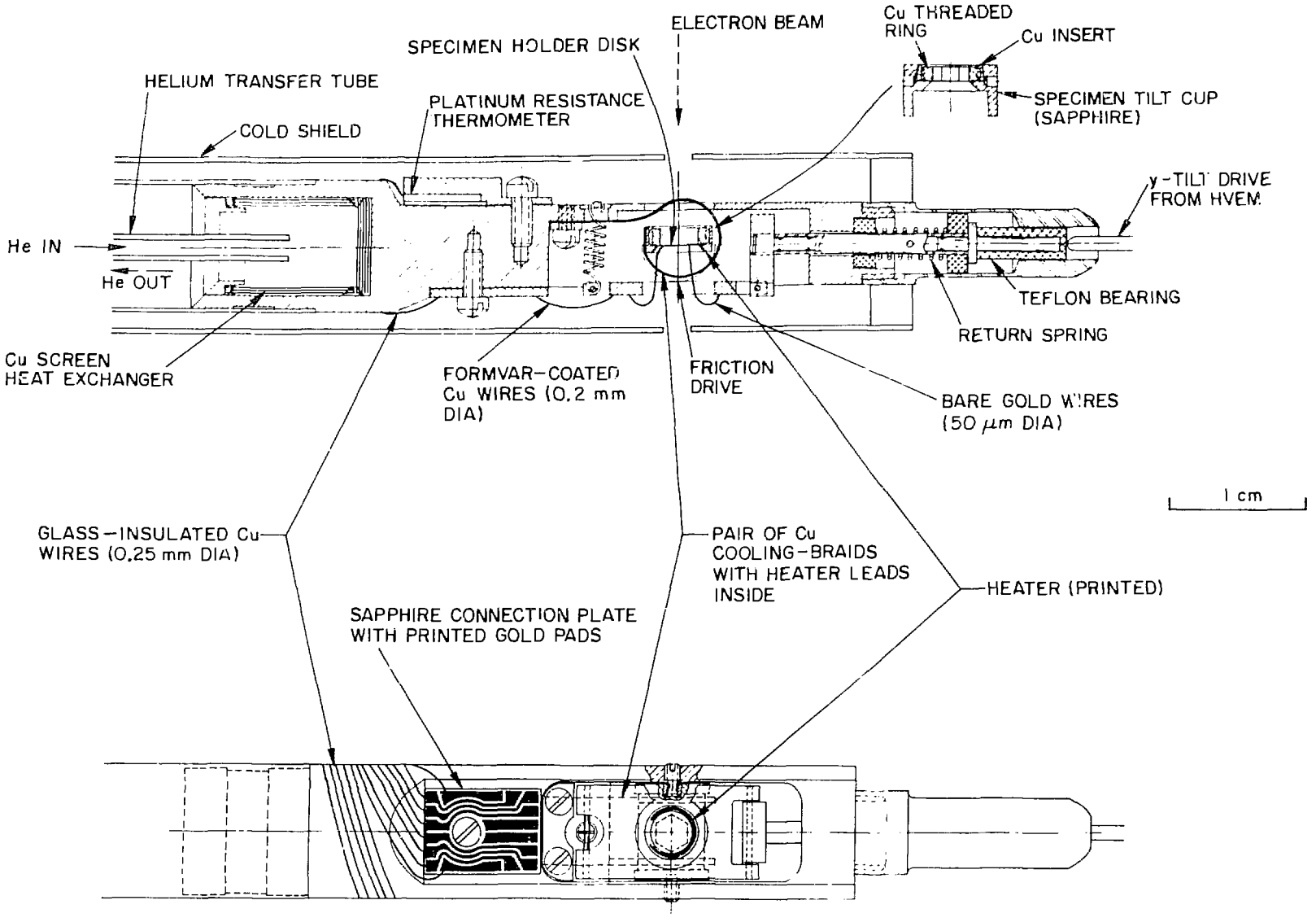
ELECTRON BEAM
Cu THREADED RING
Cu INSERT
SPECIMEN HOLDER DISK
HELIUM TRANSFER TUBE
PLATINUM RESISTANCE THERMOMETER
SPECIMEN TILT CUP (SAPPHIRE)
COLD SHIELD
y-TILT DRIVE FROM HVEM
He IN
He OUT
TEFLON BEARING
RETURN SPRING
Cu SCREEN HEAT EXCHANGER
FORMVAR-COATED Cu WIRES (0.2 mm DIA)
FRICTION DRIVE
BARE GOLD WIRES (50 μm DIA)
1 cm
GLASS-INSULATED Cu WIRES (0.25 mm DIA)
PAIR OF Cu COOLING-BRAIDS WITH HEATER LEADS INSIDE
HEATER (PRINTED)
SAPPHIRE CONNECTION PLATE WITH PRINTED GOLD PADS

Fig. 1

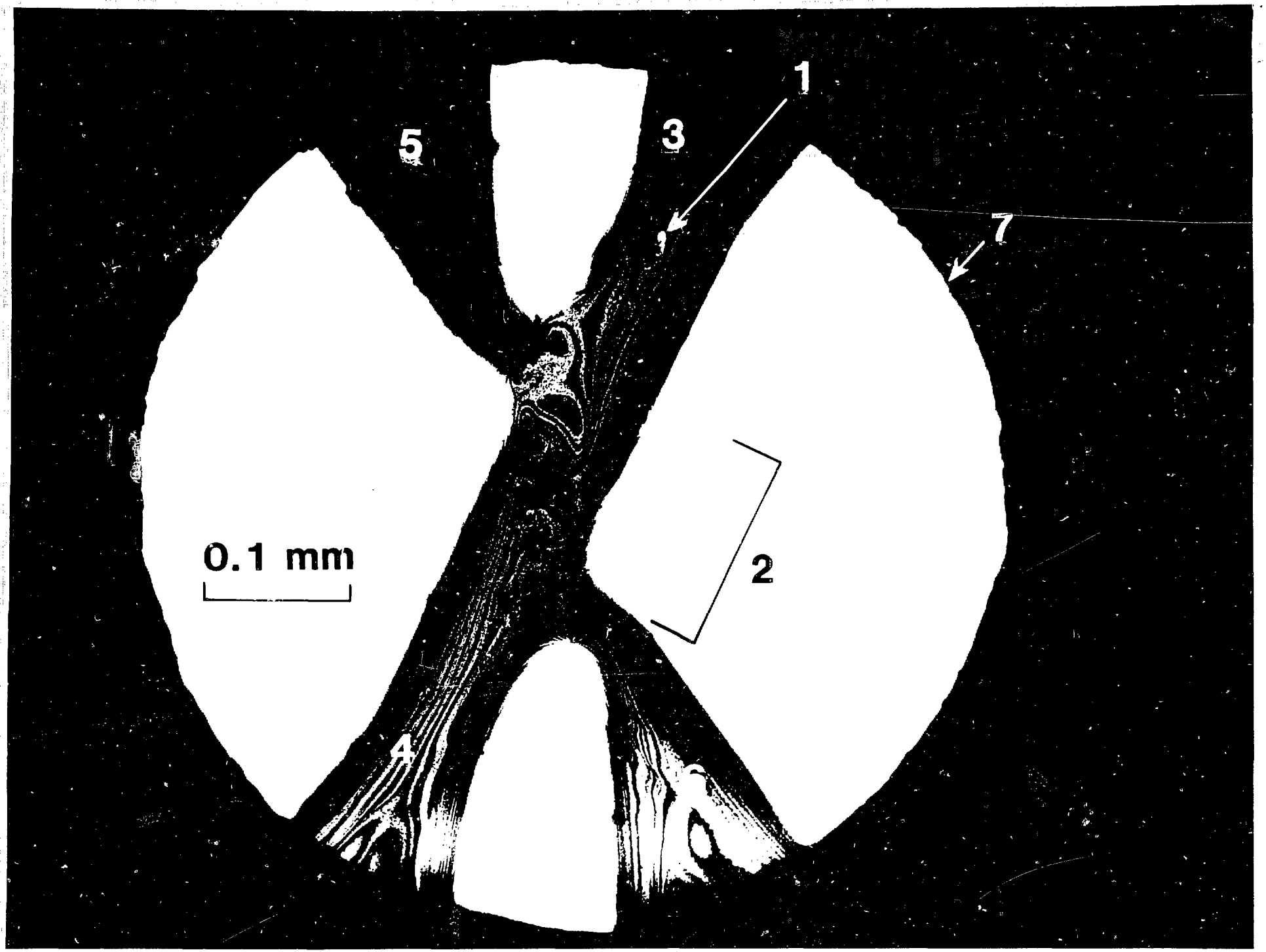
1
3
5
7
2
4
0.1 mm

Fig. 4(a)

Fig. 4(b)

Fig. 4 (c)

Fig. 4(d)

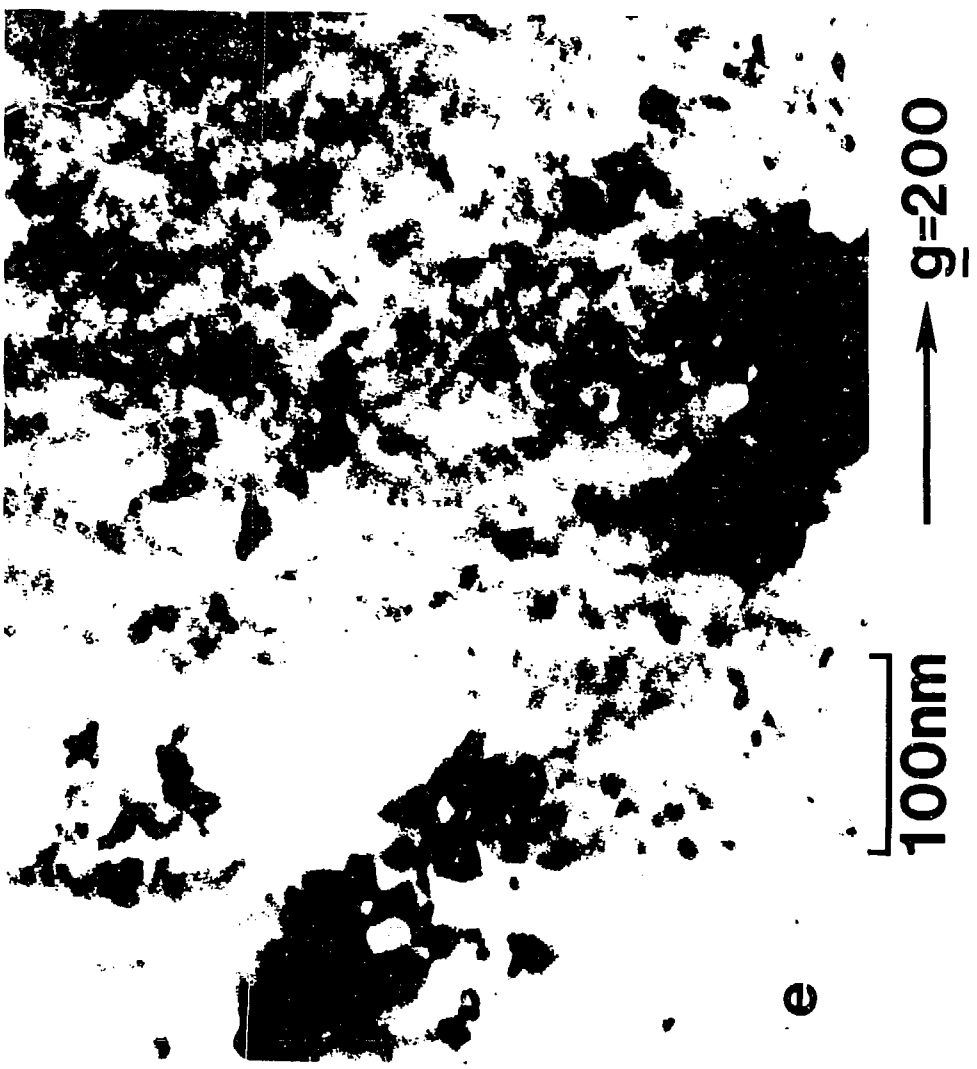

Fig. 4(e)

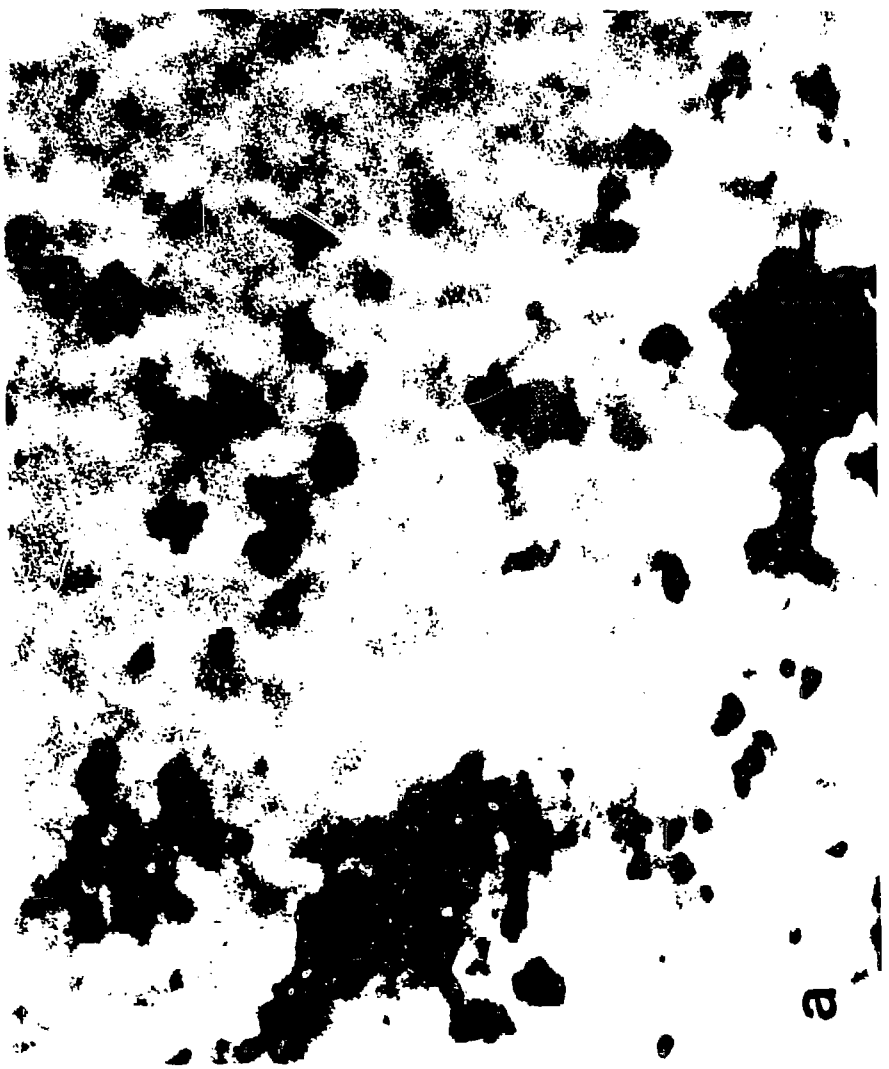

Fig. 5(a)

Fig. 5(b)

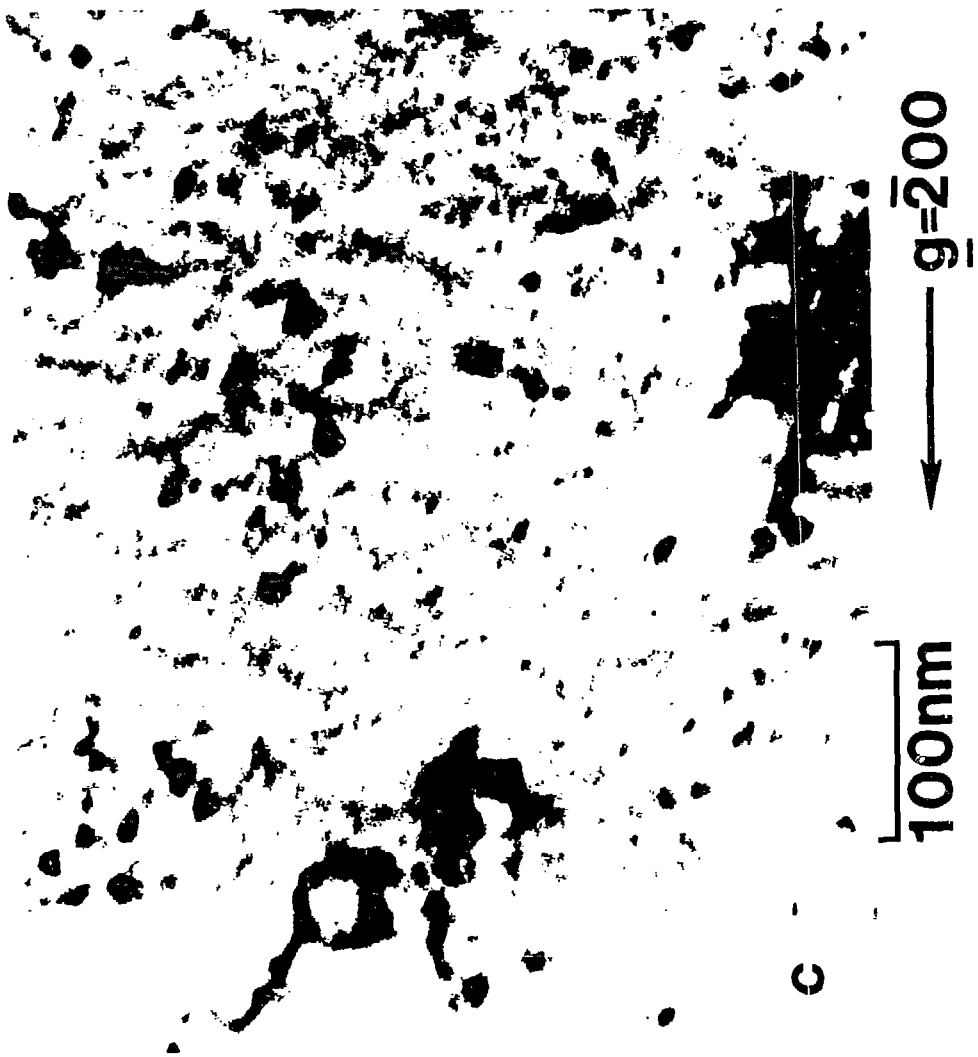

Fig. 5(c)

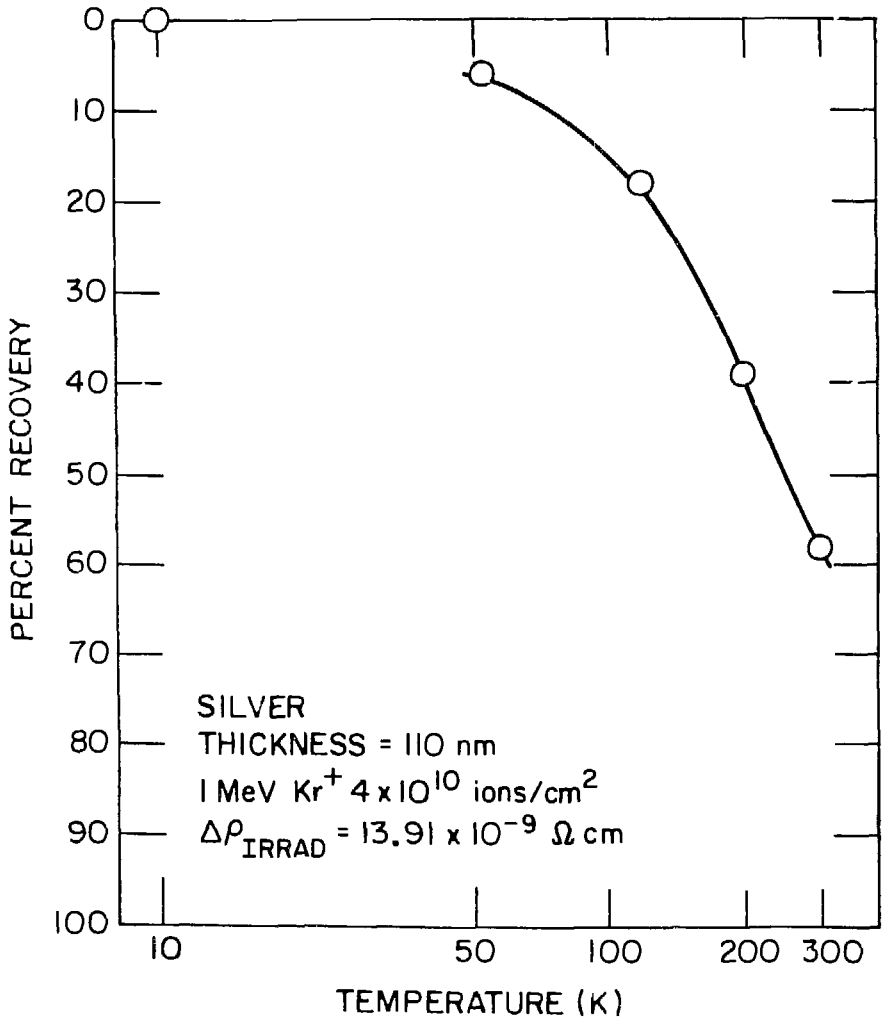
PERCENT RECOVERY
0
10
20
30
40
50
60
70
80
90
100
SILVER
THICKNESS = 110 nm
1 MeV Kr^+ 4×10^{10} ions/cm^2
$\Delta\rho_{IRRAD} = 13.91 \times 10^{-9}\ \Omega$ cm
10
50
100
200
300
TEMPERATURE (K)

Fig. 6